JOURNAL OF MATERIALS SCIENCE 31 (1996) 1053–1063

Microphase structure and calculations of the interphase in poly(styrene-b-methylphenylsiloxane) diblock copolymers: a comparative study from small-angle X-ray scattering, electron spectroscopic imaging and solid-state nuclear magnetic resonance

B. GERHARZ*, A. DU CHESNE, G. LIESER, E. W. FISCHER
Max-Planck-Institut für Polymerforschung, P.O. Box 3148, D-55021 Mainz, Germany
W. Z. CAI
Institute of Chemistry, Chinese Academy of Sciences, Beijing 100080, China

The microphase structure of a series of poly(styrene-b-methylphenylsiloxane) (PS-b-PMPS)-diblock copolymers with various compositions and molecular weights has been studied by small-angle X-ray scattering, electron spectroscopic imaging and solid-state nuclear magnetic resonance spectroscopy. This diblock copolymer system is miscible within a distinct range of temperature and molecular weight exhibiting an upper critical solution temperature. The three chosen methods which complement each other can be applied to the chemically unmodified model system. The results of the various measurements correlate to describe the microphase structure, the domain size and the interphase.

1. Introduction

Block copolymers composed from polystyrene (PS) and polydimethylsiloxane (PDMS) have been a long-standing subject of polymer science [1, 2]. These copolymers are totally immiscible and have been studied for identification of morphologies, characterization of interphases and material properties [3–5]. The system PS and polymethylphenylsiloxane (PMPS) is, in contrast to PS-b-PDMS-copolymers, a system which is partially miscible. (Fig. 1).

The diblock copolymers [6] as well as the corresponding homopolymers can be synthesized by anionic polymerization [7]. Both polymeric components are miscible with one another within a distinct range of temperature and molecular weights [8–10]. Corresponding phase diagrams have been studied by small-angle neutron scattering (SANS) and small-angle X-ray scattering (SAXS) and reveal an upper critical solution temperature [11].

Deep insight into the physics of the microphase separation was first given by Helfand [12] and Wassermann [13]. They described the microphase separation as an equilibrium of the following factors: the interaction between A and B segments is repulsive and therefore gives a driving force for growth of the domains so as to reduce the surface to volume ratio. The system has to be assumed incompressible and the block junction points will be located somewhere in the interphases. Therefore, the equilibrium morphology of the domains (size, shape, spatial arrangement of the domains and the interfacial structure) should be determined by a balance of surface to volume ratio, loss of conformational entropy and repulsive segment interaction [14].

In this paper we discuss the microphase structure and the interphase in the system PS-b-PMPS. Different methods are used to evaluate the domain size, the interphase and to characterize the microdomain morphology of chemically unmodified PS-b-PMPS.

From temperature-dependent SAXS measurements, the microphase separation transition can be detected. A combination of SAXS, differential scanning calorimetry (DSC), NMR and mechanical measurements allows the phase diagram of the system PS-b-PMPS to be described [11, 15, 16]. The partial compatibility of the homopolymers expresses itself in broad interphase regions in the block copolymers quantitatively describable by NMR measurements and also observed with DSC measurements. However, because of the very weak electron density difference

* Author to whom all correspondence should be addressed. *Present address*: Hoechst AG, Forschung Polymerisate, D-65926 Frankfurt/Main, Germany.

0022–2461

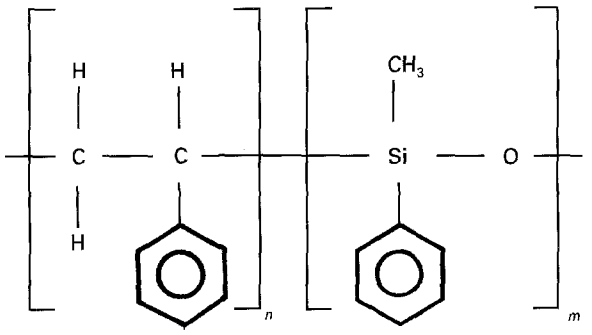

Figure 1 PS-b-PMPS.

between the components of the system PS-b-PMPS, SAXS measurements from annealed bulk samples showed only one reflection which expresses the long spacing in the microphase-separated regime [11].

Investigations using conventional TEM techniques failed to elucidate the samples morphology because of insufficient contrast between the components. Even after suppression of the contribution to the image of inelastically scattered electrons in an energy-filtering TEM (electron energy loss $\Delta E = 0$ eV) bright-field images show very low contrast owing to similar densities of the components PS and PMPS [17]. The integrated spectrometer, however, allows imaging with inelastically scattered electrons. Although contrast inverts in the inelastic imaging mode, it can be tuned and optimized as a function of sample thickness and imaging conditions. Contrast is rising from the silicon $L_{2,3}$ edge to the carbon K edge and reaches a maximum at an energy loss of $\Delta E = 270$ eV, where both phases can be clearly distinguished. Contrast improvement with increasing energy loss of the imaging electrons thus approaching the carbon absorption edge, originates from the gradual decrease of the contribution of those electrons which have interacted only with carbon (structure-sensitive contrast [18, 19]). For electrons passing through PMPS which contains silicon and oxygen, the probability of inelastic scattering occurring, leading to such energy losses, is higher. Overall intensity, however, remains very low, leading to relatively long exposure times and thus allowing the intensity differences between the phases to accumulate [17]. Elemental mapping proved that within an interval of 140 eV $< \Delta E <$ 270 eV the bright-imaged areas correspond to the siloxane phase, provided that the thickness of the samples does not exceed 100 nm [17, 20]. Exploiting structure-sensitive contrast, electron spectroscopic imaging allows direct visualization of the microphase-separated domains and their arrangement in unstained ultrathin sections of the bulk samples [17, 20–23].

Another appropriate possibility to study the phase structure of copolymers is offered by advanced solid-state NMR techniques. NMR signals of solid samples are closely related to the molecular interactions and molecular motion. For example, the NMR line shapes can be broadened by dipole–dipole interactions and anisotropic chemical shifts. On the other hand, various kinds of molecular motions can partially average these interactions, resulting in line narrowing to various extents. The NMR line shape, therefore, contains important information about the structure and molecular dynamics in the solid state.

2. Experimental procedure

2.1. Samples

A series of PS-b-PMPS diblock copolymers, as well as the homopolymer poly(methylphenylsiloxane) (PMPS) were synthesized by anionic ring-opening polymerization of 1,3,5-trimethyl-1,3,5-triphenylcyclotrisiloxane. The description of the polymerization procedure in detail and the sample characterization, are published elsewhere [6]. The composition and characterization data of the samples are given in Table I. The molecular weights were determined by membrane osmometry [6]. The glass transition temperatures were measured by DSC (Perkin–Elmer DSC7) at a heating rate of 20 K min^{-1}.

2.2. SAXS

The SAXS measurements were done using a Kratky-Camera (Anton Paar KG, Graz) with a conventional slit collimation. Data were collected using a position-sensitive detector with a resolution of 100 μm. The samples were contained in brass holders with thin polymeric windows (Bratfolie, Fa. Kalle). This allowed precise temperature control with fluctuations of less than 0.5 K.

Further data treatment involves subtraction of background scattering and accounting for the slit-type beam geometry using Strobl's desmearing algorithm [24]. In order to obtain the scattering cross-section of the samples without any arbitrary prefactors, we

TABLE I

Sample	M_n(osm)[a] (g mol^{-1})	M_w/M_n[b]	w(PMPS)[c]	Φ(PMPS)[d]	Si[e] (%)	$T_g(1)$[f] (°C)	$T_g(2)$[f] (°C)
Cp 1	60000	1.06	0.24	0.23	4.95	88	−27
Cp 2	70000	1.03	0.42	0.40	8.65	91	−27
Cp 3	60000	1.06	0.52	0.50	10.73	96	−25

[a] M_n(osm) is the total molecular weight detected with membran osmometry.
[b] M_w/M_n is the polydispersity.
[c] w(PMPS) is the weight fraction of PMPS block part.
[f] $T_g(1)$, $T_g(2)$ are glass transition temperatures for styrene block part (1) and siloxane block part (2) measured by DSC.
[d] Φ(PMPS) is the volume fraction of the PMPS block part at room temperature.
[e] Si(%) is the silicon content of the samples detected with elemental analysis.

measured the intensity of the incoming beam with a moving slit device (Paar).

The radiation source was a copper anode operated by a Siemens generator (Kristalloflex 710H), at a wavelength $\lambda = 0.154$ nm using CuK_α radiation. The K_β contribution was reduced using a nickel filter. In an accessible scattering angle interval of $0.15° \leqslant 2\theta \leqslant 4.2°$ we covered a range of wave vector $q = (4\pi/\lambda)\sin\theta$ between 0.1 and 3 nm^{-1}. A typical experiment involved heating the sample from 303–493 K and measuring the elastic scattered intensity profile at intervals of 10 K. The copolymers were allowed to equilibrate for 10 min at each measuring time to obtain profiles with good statistical quality. Measurements were then repeated during a cooling cycle to test the reversibility.

In preparation for SAXS measurements, the diblock copolymer samples were melt-pressed into a form of 1 mm × 5 mm × 25 mm under a force of 8 kN at 30 K above the glass transition temperature of the styrene phase. They were then melted directly into the Kratky sample holder at 450 K under vacuum for 10–16 h until all voids were removed. These samples were slowly cooled to room temperature in order to ensure the development of the microphase structure.

2.3. Electron microscopy

To obtain results comparable to those of the SAXS experiments, ultrathin sections were prepared directly from the same bulk samples after SAXS measurements were terminated. Keeping the sample morphologies unaffected requires sectioning at temperatures below the glass transition of the PMPS component. A Reichert Ultracut E ultramicrotome equipped with a diamond knife and a FC-4E cryo attachment was used for cryosectioning. Ultrathin sections were obtained at sample and knife temperatures of -45 and -40 °C, respectively, at a sectioning rate of 1.0 mm s^{-1}. The sections were floated off the knife on to a DMSO/H_2O mixture (60:40) and subsequently transferred to hexagonal 600 mesh copper grids. No further preparation was carried out.

Transmission electron microscopic investigation of unstained samples was performed in a Zeiss EM902-A which was operated at 80 kV. This transmission electron microscope is equipped with an integrated electron energy loss spectrometer. The selector slit in the energy dispersive plane was aligned to 20 eV in width; the objective aperture used was 8 mrad.

The micrographs were recorded on Ilford 584 Pan F photographic film. No background subtraction, contrast deepening or Fourier-filtering was employed. Micrographs represent inelastic dark-field images at $\Delta E = 270$ eV (structure-sensitive contrast), in which the PMPS and the PS phases occur bright and dark, respectively.

2.4. NMR measurements

^1H and ^{13}C NMR spectra were recorded on a Bruker MSL-300 NMR spectrometer equipped with a standard Bruker cross-polarization and magic angle spinning (CPMAS) probe head. All samples were spun at frequencies of approximately 4 kHz. The 90° pulse lengths were in the range 3.4–3.8 μs. During the detection of the ^{13}C magnetization, dipolar decoupling (DD) and total suppression of sidebands (TOSS) techniques were used to eliminate the strong ^{13}C–^1H dipolar coupling, and the spinning sidebands, respectively. The dipolar filter is described elsewhere [25], the wideline separation (WISE) hetero nuclear pulse sequence is discussed in detail by Schmidt-Rohr *et al.* [5]. All chemical shifts (^1H and ^{13}C) are given relative to tetramethylsilane (TMS).

3. Results

3.1. SAXS

The diblock copolymer system PS-b-PMPS exhibits a UCST. The system is disordered up to higher molecular weights compared to the classical systems of PS and polyisoprene (PI) or polybutadiene (PB). Also the PS-b-PMPS system exhibits higher thermostability and better electron-density contrast. Therefore, it is possible to examine the phase behaviour of the diblock copolymers by SAXS. A successful theoretical concept for the temperature dependence of the scattering pattern structure factor in the homogeneous phase was evaluated by Leibler [26]. Within this meanfield concept, polydispersity may be taken into account [27, 28]. At higher temperatures, the chosen diblock copolymers, see Fig. 2, are in the disordered (homogeneous) state, which will be discussed elsewhere [29]. By lowering the temperature, phase transition to the ordered state occurs. In contrast to polymer blends and due to the chemical connection of the different blocks in the copolymers, microscopic phases are developed after the transition from the one-phase region (microphase separation transition, MST). Values for the phase transition of diblock copolymers expressed in terms of χN (the interaction parameter, χ, times the degree of polymerization, N) can be calculated within Leiblers random-phase approximation [26]. Recently, fluctuation corrections to the mean-field expression for $(\chi N)_t$ were taken into account by Fredrickson and Helfand [28].

In the heterogeneous region, the domain formation and the interphase region were described with the help

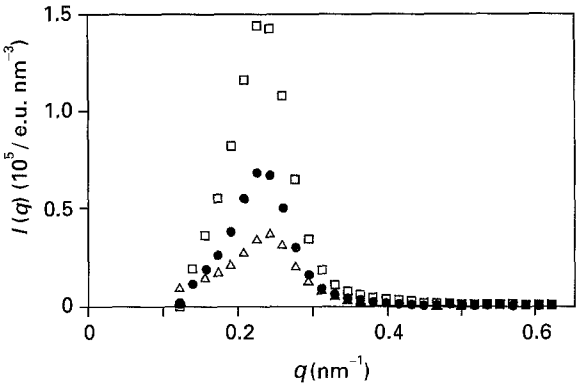

Figure 2 The scattered intensity versus scattering vector q for the sample Cp3 at three different temperatures, T: (□) 30 °C, (●) 100 °C, (△) 200 °C.

of statistical mechanics by Helfand and Wasserman [12–14]. With the functional integral representation of the partition function beyond a mean-field concept, interfacial properties were calculated by Hong and Noolandi [30–32]. The scattering function for a paracrystalline lattice was simulated by Richards and Thomason [33] in terms of a single-particle form factor and an interparticle interference term.

In principle, the scattered intensity from an ordered diblock copolymer melt can give information on the microdomain morphologies. Presuppositions are good electron-density contrast and highly oriented samples with phase boundaries as sharp as possible. Each of the samples Cp1, Cp2 and Cp3 exhibit two very broad glass transitions in the thermal analysis [6]. This suggests that at lower temperatures the samples are microphase-separated (PMPS- and PS-rich phases) and it indicates the existence of very broad interphases [6–9, 11].

Fig. 2 illustrates the temperature dependence of the experimentally determined scattering curves from sample Cp3. As the temperature is increased the maximum intensity decreases and the peak is observed to broaden, indicating a reduction in the thermodynamic interaction between the PMPS and PS-blocks. The system becomes more and more disordered [11, 26, 28].

Despite the fact that the three samples exhibit two glass transitions and a discontinuity in the plots of the reciprocal peak intensity versus reciprocal temperature (Fig. 3) (suggesting a temperature region in which a microphase-separated regime exists) every one of these samples exhibits only one SAXS maximum clearly [11, 28, 29]. Higher order Bragg peaks are not detected. Only in the case of the lamellar sample Cp3 can one observe a second-order maximum in a logarithmic plot (Fig. 4).

One may argue that the lack of more reflections is due to the destructive combination of particle form factor and interparticle interference contributions to the scattered intensity [33]. Another possibility is the weak contrast of the system [11], or that microphase separation has occurred without regular organization

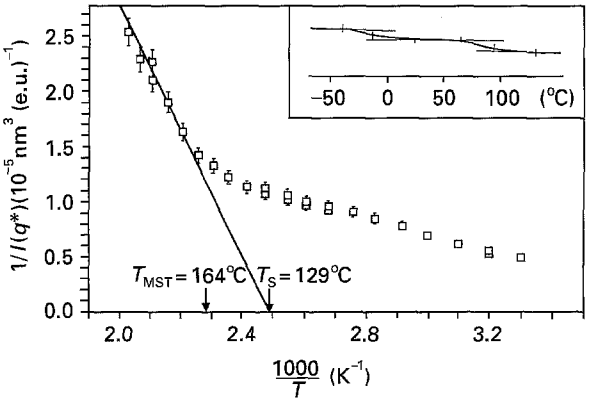

Figure 3 The inverse intensity $I(q_m^*)^{-1}$ in the maximum q^* of the diblock copolymer Cp3 versus the inverse temperature. A spinodal temperature (T_S = 129 °C) as well as a microphase-separation transition temperature (T_{MST} = 164 °C) can be determined. The insert shows the DSC measurements of the sample.

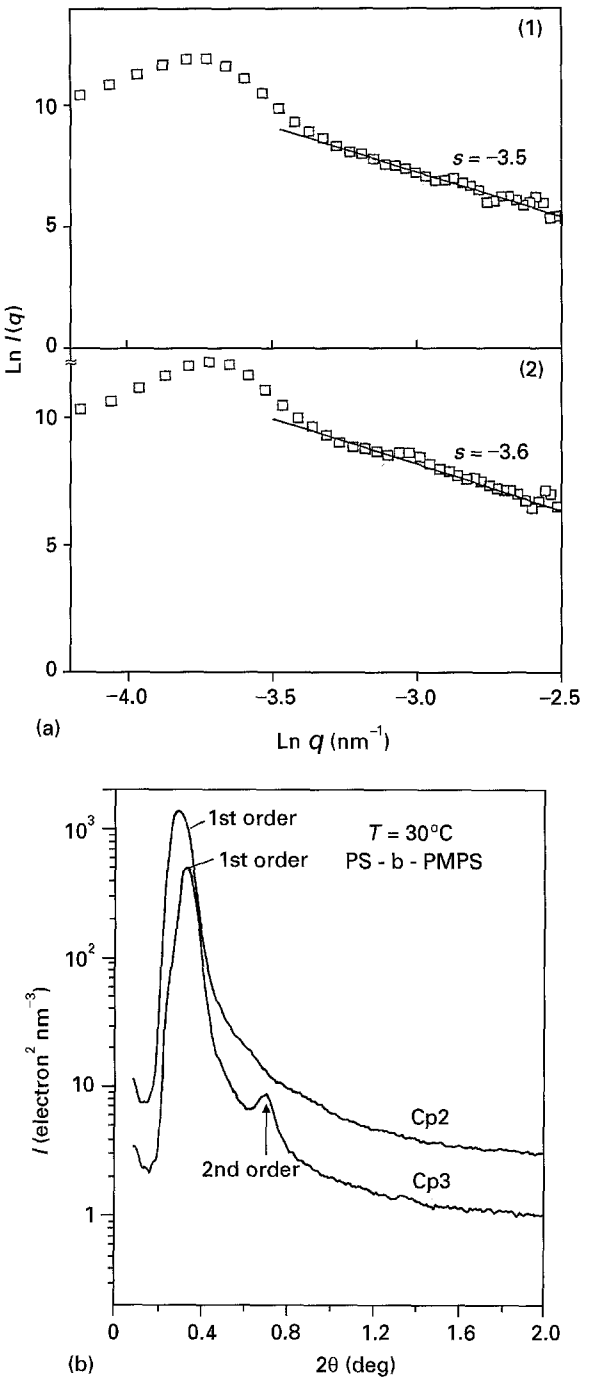

Figure 4(a) Logarithm of the scattered intensity versus logarithm of the scattering vector q at T = 30 °C for samples (1) Cp3 and (2) Cp2. The exponents can be estimated from the slope. (b) Scattered intensity versus q measured at 30 °C in mechanically oriented samples (Cp2, Cp3).

of the microdomains [34]. The last argument does not hold if we examine the electron micrographs, which exhibit excellent ordering (i.e. periodicity) (Figs 5–7). Also the preparation of highly ordered samples Cp2 and Cp3 by a mechanical shear experiment, described elsewhere [35, 36], does not result in the appearance of higher order SAXS maxima, even though a rotating anode equipment is used to obtain higher count rates and the measuring time was extended up to 24 h at each temperature (Fig. 4b).

From the first-order maximum one can calculate the long spacing given in Table II. The slope of the logarithm of the scattered intensity versus logarithm

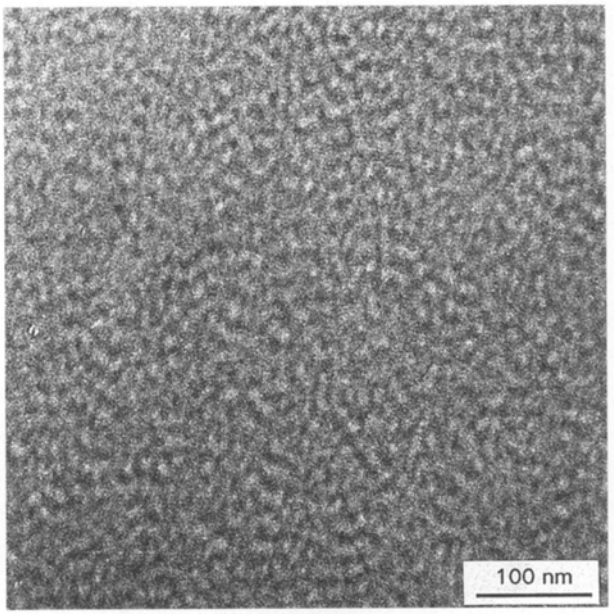

Figure 5 Electron spectroscopic micrograph at an energy loss $\Delta E = 270$ eV taken from an ultrathin section of Cp1. Bright dots correspond to PMPS spherical domains in a dark-imaged PS matrix.

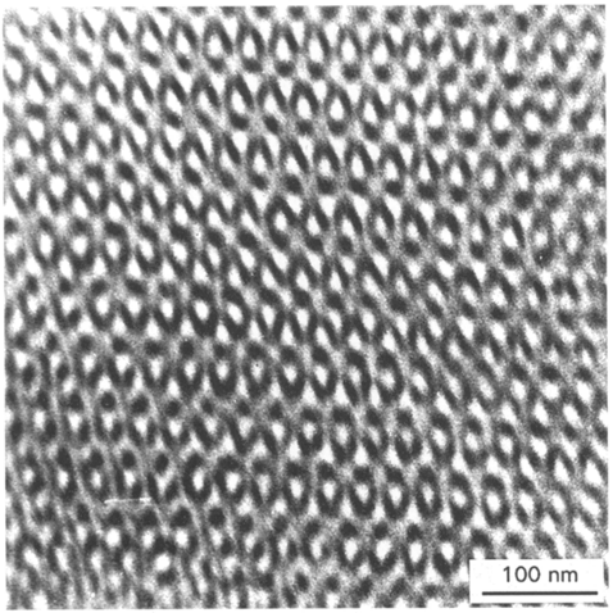

Figure 6 Electron spectroscopic micrograph at an energy loss $\Delta E = 270$ eV taken from an ultrathin section of Cp2. The highly ordered network visible is built up from bright-appearing PMPS tetrapodes (OBDD morphology). The micrograph depicts the projection almost parallel to the [1 1 1] axis, showing a distorted "wagon wheel" pattern.

of the scattering vector q (Fig. 4a) does not give any clear hint to estimate the interphases [37–39]. Therefore, a combination of SAXS measurements, solid-state NMR and electron microscopy seems useful and necessary. SAXS measurements are the superior method for detection of the microphase separation and the long spacing. Solid-state NMR is the appropriate method to supply information on the extension of microdomains and the interphase. Electron microscopy is able to elucidate the type, shape and size of the microdomains, the quality of the domain boundaries and to say whether the morphology is uniform.

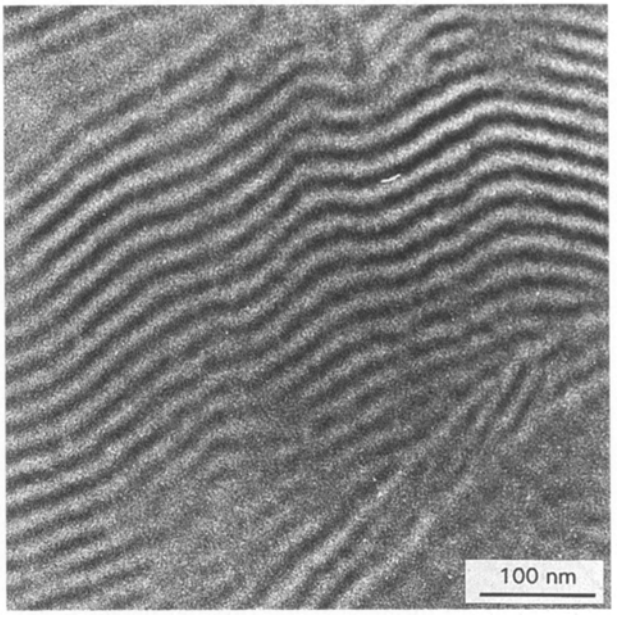

Figure 7 Electron spectroscopic micrograph at an energy loss $\Delta E = 270$ eV taken from an ultrathin section of Cp3 showing alternating lamellae.

TABLE II Domain sizes in PS-b-PMPS diblock copolymers. The observed morphologies which are predicted by theoretical calculations are characterized by EFTEM

Sample	Morphology	NMR Domain size (nm)			L_{NMR}[b]	L_{SAXS}[b]
		d_{PMPS}[a]	d_{Iph}[a]	d_{PS}[a]		
Cp 1	spherical	4.5	4.5	2.5	13–21	21
Cp 2	OBDD	6.0	4.5	2.0	14–24	27
Cp 3	lamellar	6.0	4.5	10.0	19–27	26

[a] d_{PMPS}, d_{Iph}, d_{PS} are the smallest diameter of PMPS, interphase and PS domains, respectively.
[b] L is the long period: $L_{NMR} = d_{PMPS} + 2d_{Iph} + d_{PS}$
$L_{SAXS} = 2\pi q^*$, q^* is the scattering vector at maximum intensity calculated in the temperature range of the ordered regime.

3.2. Energy filtering transmission electron microscopy (EFTEM)

Fig. 5 represents an electron micrograph taken in inelastic dark-field technique ($\Delta E = 270$ eV) from an ultrathin section of sample Cp1 (22.5 vol % PMPS). The micrograph depicts bright domains of PMPS which are assumed to be spheres in a dark PS matrix. It is difficult to associate spheres with the pattern seen on the micrograph. However, from the micrograph one can exclude cylindrical or lamellar morphologies. The pattern should be assigned to a hidden arrangement of spheres in several layers superposing each other. On the other hand, such an unordered pattern is in agreement with the observation of only one reflection in the SAXS-diagram and could be the consequence of the lack of long-range order due to non-equilibrium effects [17].

According to Leibler [26], Ohta and Kawasaki [40] and Thomas *et al.* [41], spherical domains in bulk samples of block copolymers in the equilibrium state preferentially arrange themselves in a body centred cubic lattice (B C C). The only SAXS reflection exhibited from sample Cp1 was therefore assigned to the innermost 1 1 0 reflection of a B C C lattice [17].

The amount of 22.5 vol % of the minor phase approaches the upper limit of the composition range known for the formation of a spherical microdomain morphology. The volume part of the PMPS spheres visible in the micrograph, however, does not match the composition of 22.5% by volume [17]. The "visual" volume part of the PMPS-phase can be determined with the domain radii measured from the micrographs. Identifying the d_{110} of a BCC lattice with the SAXS long spacing (20.6 nm) and with a domain radius of 6.5 nm, the volume part of the PMPS spheres visible does not exceed 6% by volume [17]. Considering an interphase of distinct thickness, this deviation from the composition of the sample will be explained below.

Different features of the morphology of sample Cp2 (39.9 vol % PMPS) as exhibited by inelastic dark-field electron micrographs ($\Delta E = 270$ eV) of ultrathin sections are shown in Fig. 6. It is obvious that the bright (PMPS) phase forms a highly ordered network. The observed structure of sample Cp2 appears to be identical to the "ordered bicontinuous double diamond" morphology (OBDD), which was analysed by Thomas *et al.* after its detection in PS-PI-star block copolymers in 1986 [42]. One year later, Hasegawa *et al.* investigated the same morphology on linear PS-PI-diblock copolymers [43]. According to these authors, and in agreement with our observations, the shape of the PMPS phase in Cp2 has to be interpreted as a double diamond lattice. Similar electron densities and partial compatibility of the components PMPS and PS in Cp2 are responsible for exhibiting only one SAXS reflection which corresponds to 27.3 nm. Taking into account structural parameters from micrographs, the latter was assigned to d_{110} of the OBDD structure which fits a tetrapode arm very well (cylinder-shaped connection between two tetrapode centres) of length 33.5 nm as derived from the micrographs [17]. As in the case of Cp1, a volume fraction of the PMPS phase was derived. The unit cell of the OBDD structure is cubic with the length of the room diagonal being equal to twice the tetrapode arm length. The diameter of the tetrapode arms differs systematically as a function of the projection of the domains with respect to the primary electron beam. In the case of the tetrapode arms lying in the image plane, their diameter amounts to 10 nm; if they are standing straight up, the diameter becomes 14.8 nm [17]. Evaluation of the PMPS volume fractions on the basis of the model of cylindrical struts first used by Thomas *et al.* [42], yields 0.18 and 0.40, respectively [17]. The model introduced in the next section will explain this discrepancy in terms of an interphase and its projections towards the electron beam as well. The OBDD morphology in block copolymers is known to occur within an interval of volume parts from 0.34–0.38. The volume part of the minor component in Cp2 (0.399) seems to be too high for the formation of the respective morphology.

Fig. 7 represents an inelastic electron micrograph ($\Delta E = 270$ eV) taken from ultrathin sections of Cp3 exhibiting a lamellar morphology (49.9 vol % PMPS). The lamellae are seen edge-on. This morphology is typical for symmetrical diblock copolymers. The SAXS measurement yields a long spacing $L_{SAXS} = 25.6$ nm. Knowing the morphology of the sample L_{SAXS} must be assigned to the average distance between lamellae consisting of the same component.

The corresponding distance between bands of the same brightness visible in the micrographs, which correspond to alternating lamellae oriented perpendicular to the image plane, does not reach the expected value of 25.6 nm. The most frequently observed long spacing is about 19 nm. This significant deviation from L_{SAXS} is explained by contraction of the ultrathin sections, which can take place in the absence of a glassy matrix. Such a contraction is limited to the liquid (PMPS) phase, which in this process becomes curved and enhances its mass thickness. This is the reason why, in the case of ultrathin sections of the lamellar sample, strong elastic contrast was observed in elastic bright-field images [17]. The surface tension of the liquid PMPS phase must be considered as the driving force for this process as well as capillary and entropic effects [17]. An additional reason for the contraction could be the irradiation damage of the specimen during exposure of the sample to electrons. Unfortunately, the contraction of the ultrathin sections does not allow further evaluations concerning the interphase in Cp3.

3.3. Solid-state NMR

Using solid-state NMR can yield information on the phase structure by probing molecular mobility. The molecular mobility of the segments in block copolymers of PS and PMPS are very different within a wide range of temperature as indicated in the difference of the glass transition temperatures (ΔT_g 130 K) for the corresponding homopolymers. This is clearly exhibited in ^{1}H wideline spectra: for the highly mobile PMPS the spectrum contains well-separated narrow lines (width of hundreds of hertz), corresponding to the protons of methyl and phenyl groups, while the PS spectrum is a featureless broad line with a width of about 40 kHz (see Fig. 11). The block copolymer spectrum deviates significantly from that which can be modelled by a superposition of the spectra of the two homopolymers and accounting for the composition. This deviation is assigned to the mutual interaction between the two blocks. The reduced mobility of the PMPS segments in the copolymers can be related to a shift of the dynamic interaction.

In order to quantify this behaviour, ^{1}H spectra of the homopolymer PMPS are shown in Fig. 8 as a function of temperature. Note the well-resolved lines requiring motions with rates exceeding 100 kHz, which are observed only at temperatures $\sim T > T_g +$ 25 K (T_g is determined by DSC) as expected from the WLF-type behaviour of amorphous polymers [44]. In order to estimate the temperature shifts of the dynamic behaviour of the PMPS-rich phase in the block copolymers, the temperature-dependent ^{1}H spectra of the copolymers were compared to that of the PMPS homopolymer. Two examples are given in Fig. 8b. From these data the shifts are estimated to be about

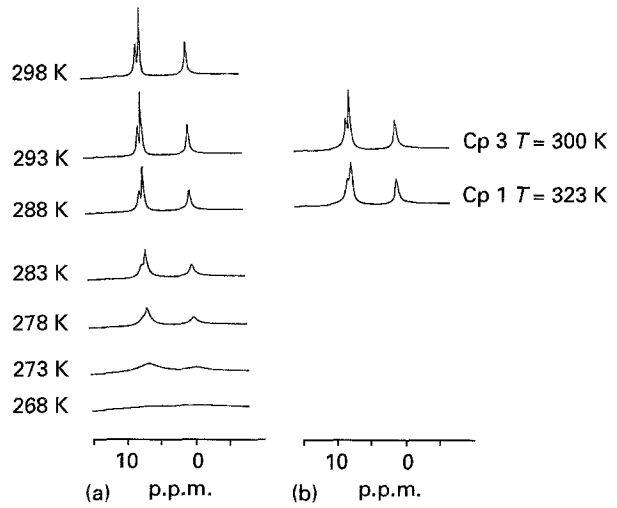

Figure 8 ^{1}H spectra at different temperatures: (a) PMPS homopolymers, (b) PMPS-b-PS copolymers Cp3 and Cp1.

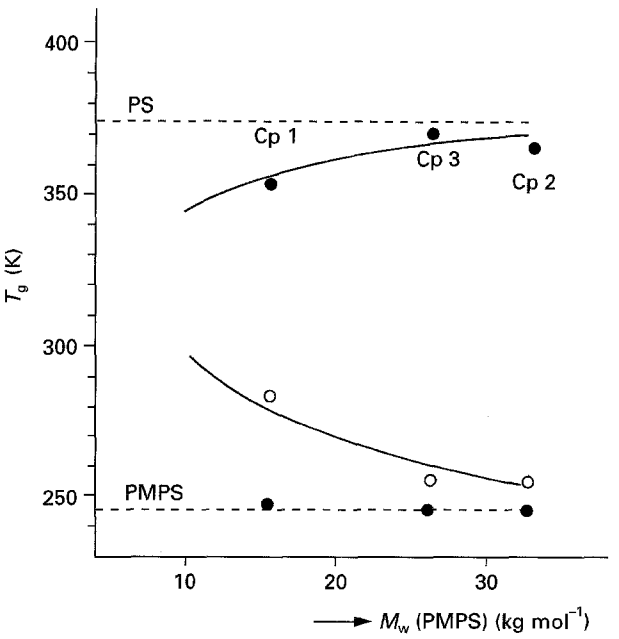

Figure 9 (○) Glass transition temperatures of PS-b-PMPS block copolymers as determined by ^{1}H NMR, plotted as a function of the molecular weight of the PMPS component. The molecular weight of the PS component is above 40–50 kg mol^{-1} in all cases. (●) DSC data are shown for comparison.

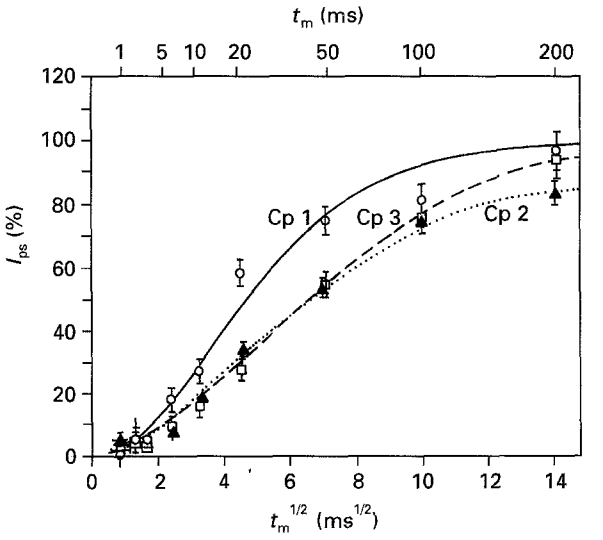

Figure 10 Spin diffusion behaviour of copolymers Cp1 , Cp2, Cp3: integrated intensity of the carbon signal for the PS backbone versus mixing time t_m. Data for sample Cp1 were taken at T = 299 K, for Cp2 and Cp3 at T = 286 K, such that the dipolar couplings (^{1}H line widths) were similar. For the selection, a dipolar filter of 6.12, 90° pulses and t_d = 19 μs were employed. (——) Theoretical fits, computed using a one-dimensional (for Cp3) or three-dimensional (for Cp1 and Cp2) diffusion model, with D_{PS} = 0.6 nm^2 ms^{-1} and D_{PMPS} = 0.05 nm^2 ms^{-1}.

10 K for copolymers Cp2 and Cp3, and about 35 K for Cp1. The lower mobility in sample Cp1 indicates the stronger interaction with PS blocks, i.e. smaller domain sizes of the PMPS-rich phase, and a higher fraction of PMPS segments within the interphase in which the components are mixed. Comparison of the temperature dependence of ^{1}H spectra from the block copolymers with that of PMPS itself (see Fig. 8) allows an estimation of the shifts of T_g. The values determined in this way and fitted under consideration of WLF dependency [44] are plotted together with those determined from DSC as a function of molecular weight of the PMPS-blocks in Fig. 9.

It is evident that DSC detects the glass transition of the phase rich in PS, which represents the larger fraction of the materials, whereas the glass transition of PMPS-rich phase is not precisely monitored. The molecular weight of the PS-block part is 40–50 kg mol^{-1} in all cases. The variation of the position of the glass transition (DSC and NMR) as a function of the molecular weight of PMPS indicates that the composition of the PS-rich and PMPS-rich phases is also changing within the series. Going to much shorter PMPS blocks will force the copolymer to a homogeneous phase with a single T_g, as is expected on the base of both phase diagrams from the corresponding homopolymers [9] and the block copolymers [11].

To determine the domain sizes in copolymers PS-b-PMPS, the dipolar filter technique [45] was used. Choosing appropriate parameters of the filter sequence, the proton magnetization of the immobile PS phase can be selectively suppressed and by this means of magnetization gradient is built up at the boundary between mobile PMPS and immobile PS phases. Subsequently, the proton magnetization in the PS phase recovers by spin diffusion from the PMPS phase during a variable mixing time, t_m. High-resolution ^{13}C spectra were recorded by transferring the proton magnetization to carbon atoms via cross-polarization after spin diffusion has taken place, in order to distinguish the signals of the different components. See Schmidt–Rohr *et al.* [45] for details. The intensity of the magnetization recovery of aliphatic carbon atoms in the PS backbone is displayed in Fig. 10 for the copolymers Cp1, Cp2, and Cp3 as a function of mixing time, t_m.

According to the diffusion theory [46], the magnetization transfer rate is determined by the spin diffusion coefficient, D, the morphology of the samples (diffusion models), and the domain sizes of the phases. In order to obtain easily comparable data, we used the same value of the diffusion coefficient, D, for all simulations. The spin diffusion data for different samples

are recorded at appropriate temperatures, where ^{1}H NMR spectra have similar line shapes. For the data shown in Fig. 10, sample Cp1 is measured at 299 K, Cp2 and Cp3 at 286 K.

With the morphology of these samples in mind from the EFTEM investigation, the spin diffusion coefficient, D, was obtained using the ^{1}H line width of the corresponding proton wideline spectra [47]. The theoretical predictions are shown in Fig. 10 as solid lines. With the expected accuracy of 20%, the domain sizes determined in this way are given in Table II. It was found that the spin diffusion rate of copolymer Cp2 is very close to that of Cp3. Therefore, the different domain sizes are due to different morphologies as observed by EFTEM.

According to the spin diffusion data, all copolymers possess a rather wide interfacial region. Note that the term interfacial region is now used to denote the region where the mobilities of both PS and PMPS segments are different from the mobilities within the domains of each more or less pure component. The spin diffusion data for all copolymers can be fitted with the same thickness for the interfacial region. By means of a novel technique (hetero nuclear two-dimensional WISE-NMR [47]), the ^{1}H NMR widelines which overlap completely in the conventional one-dimensional ^{1}H spectra, can be separated according to the chemical shifts of the corresponding carbon nuclei.

Fig. 11 shows a two-dimensional WISE-NMR spectrum of copolymer Cp2 recorded at 298 K. The signal around 41 p.p.m. along the ^{13}C dimension originates from aliphatic carbons of the PS backbone. Its broad line shape along the ^{1}H dimension indicates low mobility. On the other hand, the signal near 1 p.p.m., which corresponds to a methyl group, represents a narrow line which is typical for a very mobile component. It is noticed that this narrow peak superposes a broad base, which is attributed to methyl groups of those PMPS units which are located within the interfacial region and thus partially immobilized due to their molecular interpenetration with rigid PS segments. This broadened component of a narrow line for a mobile group is not observed in an incompatible system, such as PS-b-PDMS [48]. The NMR data suggest that the region of the PS-b-PMPS copolymers which is characterized by a mobility gradient region (interfacial region) can be as large as 4–5 nm.

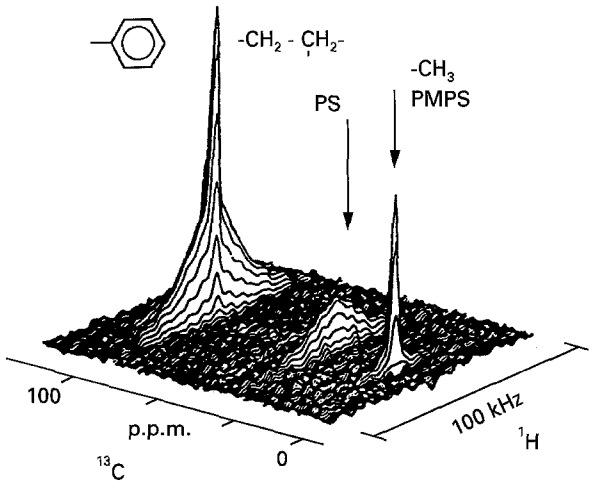

Figure 11 Heteronuclear two-dimensional WISE NMR spectrum of copolymer Cp3 at $T = 300$K.

4. Discussion

It has already been mentioned in Section 3.2 that the sizes of PMPS domains appear usually smaller in the micrographs (structure sensitive contrast) than is expected from the analysed composition if one assumes sharp phase boundaries and full visibility of the PMPS phase. Only in the case of cylindrically shaped domains oriented perpendicular to the image plane, does the domain size measured on the micrographs match the value expected from the composition. (Owing to the contraction of the ultrathin sections, the lamellar morphology is not suitable for the following consideration.) This leads to the conclusion that the domain boundaries must be described by a relatively broad interphase. The domain size which can be recognized on micrographs is a function of geometrical factors such as the orientation of the domains with respect to the beam direction. In the case of cylinders extending parallel to the electron beam (normal to the image plane) the signal due to the PMPS component in the interphase is accumulated along the whole thickness of the transmitted ultrathin section. Then the part of the interphase which is brightly imaged is wider, compared to the same cylinders oriented perpendicular to the electron beam. In the last case, the PMPS phase looks thinner because only a small part of the transmitted thickness, t, of the section consists of PMPS, which in the interphase is gradually diluted by PS. The same is valid for spherical PMPS domains. In such cases it is expected that the interphase remains invisible, as if the whole interphase would belong to the PS phase. It is therefore desirable to describe the interphase by an appropriate model. Such a model is depicted in Fig. 12 and defined as follows.

1. The interphase separates the pure PS phases from the pure PMPS phases, i.e. it extends over the area where covalent bonds between the components are accumulated. The interphase has the thickness d_{Iph}.
2. The concentration of each component averaged over the whole thickness of the interphase amounts to 50%.
3. From (2) it follows that a virtual sharp phase boundary can be defined, which divides the interphase volume into two parts of equal volume. This sharp boundary coincides with the phase boundary expected according to the composition for an interphase of thickness zero.
4. The shape of the concentration profile remains undefined.

The application of the model depends on the type of morphology: for lamellae, the interphase extends parallel to the lamellae. The virtual sharp phase boundary is right in the middle of the interphase, extending into the neighbouring domains to the same depth. However, because of the contraction of the ultrathin sections of the lamellar sample, no evaluation of the

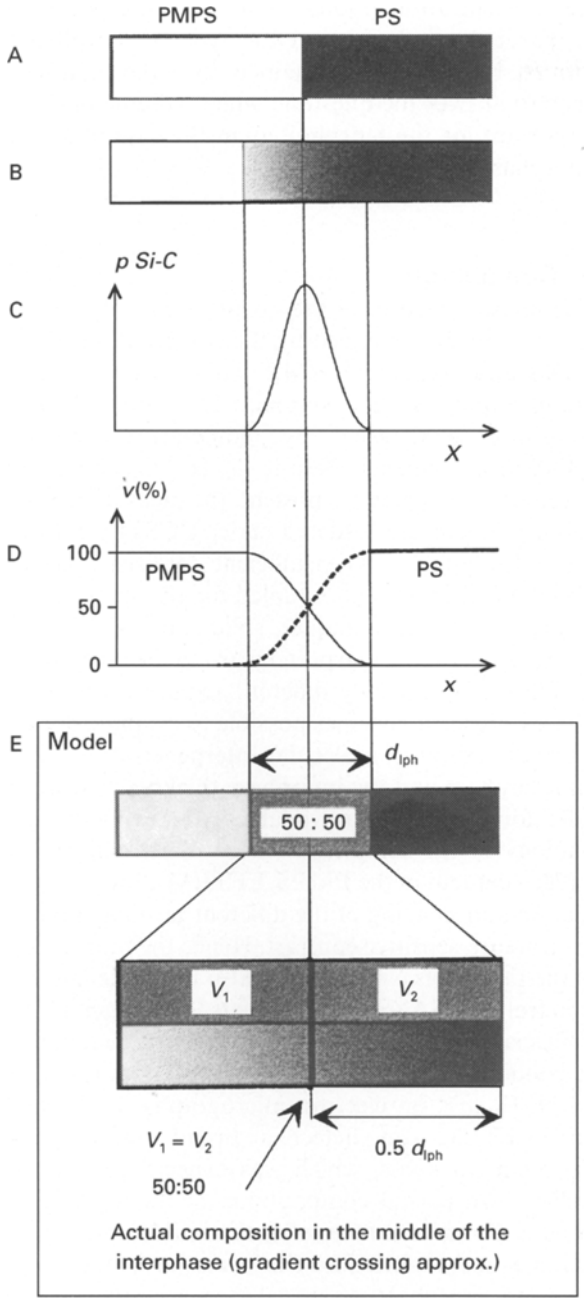

Figure 12 Schematic representation of the model used to evaluate the interphase thickness. A, imaginary sharp domain boundary; B, real domain boundary described by a continuous transition region (interphase) between the phases; C, distribution of the probability to find covalent linkages between different blocks on axis x which extends normal to the domain boundary; D, gradients of the volume content of the components along the x-axis (the given case is for a symmetrical block copolymer); E, the models introduced (see text).

interphase was carried out. In the case of cylindrically shaped domains the interphase is parallel to the surface of the cylinder reaching deeper into the dispersed domain (cylinder) than in the matrix, because the occupied volume, V, per radius, r, is dependent on r^2. If domains are spherical the same as above is valid, but with a cubic dependency. Thus an interphase thickness can be evaluated using

$$d_{\mathrm{Iph}} = (2r_{\mathrm{th}}^2 - r_{\mathrm{vis}}^2)^{1/2} - r_{\mathrm{vis}} \quad (1)$$

and

$$d_{\mathrm{Iph}} = (2r_{\mathrm{th}}^3 - r_{\mathrm{vis}}^3)^{1/3} - r_{\mathrm{vis}} \quad (2)$$

TABLE III Unit cell volume, macroscopic volume part, Φ_{th}, visible domain radius, r_{vis}, and corresponding volume part for Cp1 and Cp2. The visible domain sizes are measured from electron micrographs (structure-sensitive contrast at $\Delta E = 270$ eV, for Cp2 the radius of the tetrapode arms lying in the image plane is given). d_{Iph} is the thickness of the interphase as evaluated (see text). The radius $r_{50:50}$ gives the position of the 50:50 surface, extending in the middle of the interphase where its composition is 50:50 (gradient crossing approximation). $\Phi_{50:50}$ is the volume part of the dispersed phase enclosed by the 50:50 surface

Polymer	$\Phi_{\mathrm{th.}}$	Unit cell vol. (10^4nm^3)	$r_{\mathrm{th.}}$ (nm)	$r_{\mathrm{vis.}}$ (nm)	$\Phi_{\mathrm{vis.}}$	d_{Iph} (nm)	$r_{50:50}$ (nm)	$\Phi_{50:50}$
Cp1	0.225	2.47	8.7	5.5	0.056	4.98	7.99	0.173
Cp2	0.399	5.78	7.4	5.0	0.183	4.19	7.09	0.366

for cylindrical and spherical domains, respectively. The subscript *th* indicates the domain radius which is expected according to the composition for sharp phase boundaries, vis denotes the radius which is measured on the micrographs (cylinders are lying in the image plane). The results are given in Table III. It turns out, that they are in excellent agreement with those from the NMR measurements. This demonstrates that the previous assumption, i.e. that the interphase is imaged differently depending on the orientation with respect to the beam, and the supposed model for the interphase, describe the real circumstances well. This leads to an interesting question concerning the formation of equilibrium morphologies as a function of composition and interphase thickness. Cp1, having a PMPS volume fraction of 0.225, exhibits spherical PMPS domains and was shown to have an interphase of nearly 5 nm. PS-b-Pl of a comparable degree of polymerization at this composition shows a cylindrical morphology and has a narrow interphase [14, 49]. In analogy, Cp3 possess a PMPS volume fraction of 0.399 but shows the OBDD–morphology which is known to occur within a narrow composition interval of 0.34–0.38 [43, 49].

The following discussion represents an unconventional attempt to explain these discrepancies. The domains of microphase-separated polymers are limited by phase boundaries of high energy. Hence the approach to thermodynamic equilibrium minimizes the surface-to-volume ratio of the separating phases within the boundary conditions of composition, incompressibility and block lengths. Under these restrictions, block copolymers form microdomains of various morphologies which are strongly dependent on the volume fractions of the immiscible components [14]. In terms of our model, suggesting thick interphases, the question arises, which room dividing surface, extending between the phases, is minimized? It is reasonable to expect that this is the surface of highest energy where mixing of the components is at its maximum, i.e. at the surface where the gradients of both components are crossing and the composition is 50:50. In the case of symmetrical block copolymers with uncurved domain boundaries (lamellae) this happens in the geometrical middle of the interphase. For curved interphases, the 50:50 volume boundary is

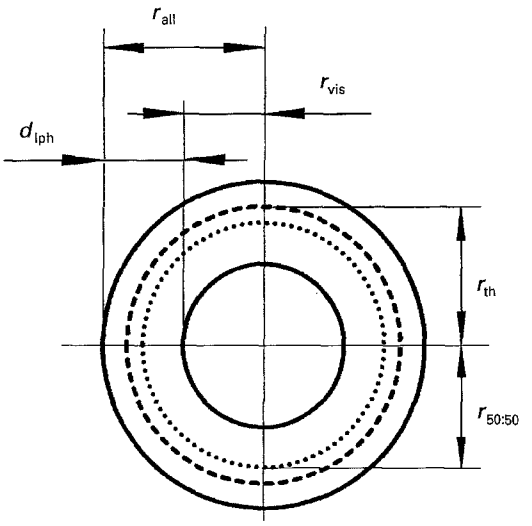

Figure 13 Schematic representation of a section through a domain of the dispersed phase PMPS. r_{vis}, the visible domain radius; r_{th}, the domain radius which is expected according to macroscopic composition and considering sharp phase boundaries. $r_{50:50}$ is the radius denoting the middle of the interphase. d_{Iph} represents the interphase thickness.

shifted away from the geometrical centre of the projected interphase defined by $r_{50:50}$. For the sake of simplification we make the approximation that in all the cases the gradients cross each other in the geometrical middle of the interphase (gradients crossing approximation, Fig. 13).

The domain radii and the interphase thickness considered in the model depicted in Fig. 12 are related to the following volume parts:

1. radius, r_{th}, of the dispersed phase with the analysed (macroscopic) volume part, Φ_{th};
2. thickness, d_{Iph}, of the interphase (invisible) with a volume fraction, Φ_{Iph};
3. radius, r_{vis}, of the visible (pure) dispersed phase with volume fraction $\Phi_{vis} = \Phi_{th} - 0.5\,\Phi_{Iph}$;
4. radius, r_{all}, of the dispersed phase including all the interphase with a volume part $\Phi_{all} = \Phi_{th} + 0.5\,\Phi_{Iph}$;
5. $r_{50:50}$ in the middle of the interphase were the 50:50 surface extends enclosing a volume fraction $\Phi_{50:50}$.

For lamellar structures, $\Phi_{50:50}$ equals Φ_{th}. Applying the same consideration on cylinders or spheres it results that the volume ($\Phi_{50:50}$) enclosed by the 50:50 surface is always smaller than the corresponding macroscopic volume fraction of the dispersed component. The results are given in Table III. Whereas the macroscopic volume parts Φ_{th} for both Cp1 and Cp2 seem to be too high for the formation of the respective morphologies, $\Phi_{50:50}$ of Cp1 occurs to be inside the volume part interval required for the spherical morphology in the narrow phase approximation [13]. In analogy, $\Phi_{50:50}$ of Cp2 coincides with the values of the volume parts at which the OBDD morphology is reported to occur in systems exhibiting a narrow interphase [42, 43, 49]. Note that for the OBDD morphology this interval is very small. Surely, the simple geometric model used is not suitable to describe the real concentration gradient within the interphase and its particular influence on the type of morphology formed, but the results obtained show the right tendency to answer the question: which volume parts are important for the morphology in the case of a thick interphase?

5. Conclusion

The phase structure of the investigated polymer system can be characterized by the combination of ESI, SAXS and solid-state NMR without any chemical modification of the system. The order–disorder transition is detected by temperature-dependent SAXS measurements. Despite the fact that highly ordered morphologies are present, the measurements at room temperature (ordered state, UCST) yield only one reflection due to insufficient contrast. Conventional TEM investigation failed for the same reason. Using advanced techniques, solid-state NMR yields information on the morphology using the difference in mobility of chemically different segments within the phases. Hence it becomes possible to evaluate domain sizes, the extent of molecular interpenetration within an interphase and the interphase thickness. However, full information is only available by knowing the morphology of the samples. Because of the silicon and oxygen content in the PMPS, EFTEM allows discrimination and imaging of the different unstained phases in structure-sensitive contrast. Hence the morphology of the samples is elucidated by also using the information from the SAXS measurements (long spacing). The long spacings obtained with the different methods are in good agreement, as are the domain sizes measured by NMR and on electron micrographs. Both NMR and EFTEM can detect a broad interphase of 4.2–5 nm thickness, which was expected due to the well-known partial compatibility of the investigated system. Compared to totally immiscible systems, the volume parts required for the formation of the corresponding morphology are shifted slightly towards higher values for the dispersed phase. This shift is explained as an effect of mixing within the interphase and evaluated using a simple geometric model.

Acknowledgements

The authors are indebted to G. Urban, U. Wiesner, H. W. Spieß and G. Wegner for helpful discussions. Financial support of the German Ministry for Scientific Research is gratefully acknowledged.

References

1. T. C. KENDRICK, B. M. PARBHOO and J. W. WHITE, in "Comprehensive Polymer Science", edited by G. Allen and J. C. Bevington (Pergamon Press, Oxford, 1989) p. 459.
2. I. YILGOR and J. E. McGRATH, *Adv. Polym. Sci.* **86** (1988) 1.
3. S. KRAUSE, M. ISKANDAR and M. IGBAL, *Macromolecules* **15** (1982) 105.
4. B. WANG and S. KRAUSE, *ibid.* **20** (1987) 2201.
5. K. SCHMIDT-ROHR, J. CLAUSS and H.W. SPIESS, *ibid.* **25** (1992) 3273.

6. B. GERHARZ, TH. WAGNER, M. BALLAUFF and E.W. FISCHER, *Polymer* **33** (1992) 3531.
7. B. MOMPER, TH. WAGNER, U. MASCHKE, M. BALLAUFF and E.W. FISCHER, *Polym. Commun.* **31** (1990) 186.
8. S. NOJIMA and T. NOSE, *Polym. J.* **14** (1982) 269.
9. U. MURSCHALL, E.W. FISCHER, CH. HERKT-MAETZKY and G. FYTAS, *J. Polym. Sci. C Polym. Lett.* **24** (1986) 191.
10. T. SHIONI, T. HAMADA, M. MIHARCHI, T. NASAKI and A. NAKAJIMA, *Polymer* **31** (1990) 448.
11. B. GERHARZ, PhD thesis, 55128 Mainz (1991).
12. E. HELFAND, *Macromolecules* **8** (1975) 552.
13. E. HELFAND and Z. R. WASSERMAN, *ibid.* **11** (1978) 960.
14. *Idem*, "Development in Blockcopolymers I, II", edited by I. Goodman (Applied Science, New York, 1982) p. 99.
15. W. Z. CAI, K. SCHIMIDT-ROHR, N. EGGER, B. GERHARZ and H.W. SPIESS, *Polymer* **34** (1993) 267.
16. H. W. SPIESS, *Angew. Makromol. Chem.* 202/203 (1992) 331.
17. A. DU CHESNE, PhD thesis, University of Mainz (1993).
18. L. REIMER, in "Energy Filtering TEM", edited by P. W. Hawkes, Advances in Electronics and Electron Physics 81, (Academic Press Boston, San Diego, New York, London, Sydney, Tokyo, Toronto, 1991) p. 67.
19. L. REIMER and M. ROSS-MESSEMER, *J. Microsc.* **159** (1990) 143.
20. A. DU CHESNE, G. LIESER and G. WEGNER, in "Electron Microscopy" Vol. I, edited by A. Rios, J. M. Arias, L. Megías-Megías and A. López (Secretariado de Publicaciones, University of Granada, 1992) p. 255.
21. A. DU CHESNE, G. LIESER and G. WEGNER, Colloid & Polym. Sci. **272** (1994) 1329.
22. *Idem*, "Paper presented at the 4th European Workshop on ESI, Diffraction and Analysis Techniques", Münster, 1993, Unpublished.
23. A. DU CHESNE, B. GERHARZ, G. LIESER and G. WEGNER, in preparation.
24. G.R. STROBL, *Acta Crystallogr.* **A26** (1970) 367.
25. N. EGGER, K. SCHMIDT-ROHR, B. BLÜMICH, W.-D. DOMKE and B. STAPP, *J. Appl. Polym. Sci.* **44** (1992) 289.
26. L. LEIBLER, *Macromolecules* **13** (1980) 1602.
27. C. BURGER, W. RULAND and A.N. SEMENOV, *ibid.* **23** (1990) 3339.
28. G. H. FREDRICKSON and E. HELFAND *J. Chem. Phys.* **87** (1987) 697.
29. B. GERHARZ, G. URBAN, T. PAKULA, G. MEIER and E. W. FISCHER, in preparation.
30. K.H. HONG and J. NOOLANDI, *Macromolecules* **17** (1984) 1531.
31. *Idem, ibid.* **14** (1981) 727.
32. *Idem, ibid.* **14** (1981) 1231.
33. R.W. RICHARDS and TZ.L. THOMASON, *ibid.* **16** (1983) 982.
34. R. MAYER, *Polymer* **15** (1974) 137.
35. G. HADZIIOUANNOU, A. MATTIS and A. SKOULIOS, *Coll. Polym. Sci.* **15** (1979) 257.
36. K. ALMDALE, F.S. BATES and K. MORTENSEN, *J. Chem. Phys.* **96** (1992) 9122.
37. W. RULAND, *Macromolecules* **20** (1987) 87.
38. W.G. JUNG and E.W. FISCHER, *Makromol. Chem. Makromol. Symp.* **16** (1988) 281.
39. F. ANNIGHÖFER and W. GRONSKI, *Makromol. Chem.* **185** (1984) 2213.
40. T. OHTA and K. KAWASAKI, *Macromolecules* **19** (1986) 2621.
41. E. L. THOMAS, D. J. KINNING, D. B. ALWARD and C. S. HENKEE, *ibid.* **20** (1987) 2934.
42. E. L. THOMAS, D. B. ALWARD, D. J. KINNING, D. C. MARTIN, D. L. HANDLIN Jr and L.J. FETTERS, *ibid.* **19** (1986) 2197.
43. H. HASEGAWA, H. TANAKA, K. YAMASAKI and T. HASHIMOTO, *ibid.* **20** (1987) 2940.
44. J.D. FERRY, in "Viscoelastic Properties of Polymers" (Wiley, New York, 1980).
45. K. SCHMIDT-ROHR, J. CLAUSS, B. BLÜMICH and H.W. SPIESS, *Magn. Reson. Chem.* **28** (1990) 3.
46. *Idem, Polym Prep. ACS Div. Polym. Chem.* **31** (1990) 172.
47. K. SCHIMIDT-ROHR, J. CLAUSS and H. W. SPIESS, *Acta Polym.* **44** (1993) 1.
48. M. BLOEMBERGEN, *Physica* **15** (1949) 386.
49. F. S. BATES and G. H. FREDRICKSON, *Ann. Rev. Phys. Chem.* **41** (1990) 525.

Received 15 April 1994
and accepted 24 May 1995